J. Fluid Mech. (1997), *vol.* 344, *pp.* 67–94. Printed in the United Kingdom

Instability of a two-dimensional plane wall jet subjected to blowing or suction

By MICHAEL AMITAY AND JACOB COHEN

Faculty of Aerospace Engineering, Technion – Israel Institute of Technology, Haifa 32000, Israel

(Received 17 March 1996 and in revised form 3 December 1996)

The effects of wall blowing or suction on the stability characteristics of a laminar incompressible two-dimensional plane wall jet are investigated both experimentally and theoretically. A quantitative comparison between linear stability calculations and phase-locked experimental data, obtained when the wall jet is subjected to two-dimensional excitations, confirms the co-existence of the viscous and inviscid instability modes and the theoretically predicted effects of blowing and suction on the stability of the wall jet. According to these predicted effects, blowing stabilizes the inviscid mode while destabilizing the viscous one; suction has the opposite effect. Furthermore, blowing and suction tend to increase and decrease, respectively, the ratio between the outer and inner amplitude maxima of the streamwise velocity fluctuation. When wall blowing is applied, the instability domain is enlarged and includes higher-frequency waves. In addition, the region where both unstable modes co-exist simultaneously begins at a lower local Reynolds number. Opposite effects are caused when suction is applied. The quantitative comparison between the theory and experiment includes the cross-stream structure and the downstream growth of the streamwise velocity fluctuations. In order to accurately account for the effect of the mean flow divergence in the stability analysis, the second-order corrections to the mean flow solutions are obtained for all wall conditions. Spectral distributions, obtained when natural wall-jets are subjected to blowing and suction, support qualitatively the above results.

1. Introduction

In this work, the laminar-to-turbulent transition of a two-dimensional wall jet is investigated. A wall jet is a thin jet of fluid that flows tangentially to a wall. It consists of an inner region wherein the flow resembles the conventional wall boundary layer and an outer region wherein the flow is like a free shear layer. The wall jet is of considerable technological importance for applications like vertical take-off aircraft, airfoil design, electronic cooling and paint spray. Owing to the low critical Reynolds number, the flows in most applications are turbulent. Nevertheless, in some applications (e.g. effective cooling) a controllable location of transition to turbulence is required.

The mean flow of a laminar plane wall jet was first examined theoretically by Tetervin (1948). By numerical integration of the governing equations, he obtained a self-similar solution and predicted that the wall-jet thickness would increase as the 3/4 power of the downstream distance and that the velocity would decrease inversely as the 1/2 power of the downstream distance. A similar mathematical solution, obtained

in a closed analytical form, was later presented independently by Akatnov (1953) and Glauert (1956). In addition, in a subsequent paper, Glauert (1958) showed that an arbitrary distance can be added to the downstream coordinate without altering the solution, which amounts to a shift of the virtual origin in the case of the plane wall jet.

The temporal linear stability of a wall jet subjected to small wavy disturbances was examined theoretically by Chun & Schwarz (1967). By solving the Orr–Sommerfeld equation they showed that the critical local Reynolds number, R_{cr}, which is based on the local boundary layer thickness and the local maximum velocity, is 57. They also revealed the existence of a second unstable mode at higher Reynolds numbers.

Using hot-wire measurements in an air wall jet, Bajura & Szewczyk (1970) confirmed experimentally the theoretical findings of Tetervin, Akatnov and Glauert. Furthermore, by subjecting the wall jet to two-dimensional excitations, they showed that in the disturbance amplitude distribution there are two large peaks located in the inner and outer regions of the wall jet. Since the amplification rate of the outer peak was larger than that of the inner one, they concluded that the instability of the whole jet is controlled by the outer region.

The dominance of the outer region was also reported by Bajura & Catalano (1975), who investigated experimentally the transition to turbulence in two-dimensional plane wall jets, using flow visualization in a water tunnel. They observed the following stages in natural transition: (i) formation of discrete vortices in the outer shear layer; (ii) coalescence of adjacent vortices in the outer region, coupled with the rolling up of the inner shear layer; (iii) eruption of the wall jet off the surface of the flat plate into the ambient fluid (the lift-off stage); (iv) dispersion of the organized flow pattern by three-dimensional turbulent motions; and (v) re-laminarization of the upstream flow, until another vortex pairing occurs. Their investigation showed that the initial stages of transition are two-dimensional in nature, and are dominated by the mechanism of vortex pairing, which is commonly observed in free shear flows. By subjecting the wall jet to acoustic disturbances, they found that the forced transition is essentially similar to natural transition, except for the elimination of the downstream intermittency and the establishment of a fixed downstream location for transition.

The generation of the double-row vortical structure in the near field of a plane wall jet was recently investigated experimentally by Hsiao & Sheu (1994) using flow visualization and hot-wire measurements. They found that the induction of a secondary vortex in the inner region is caused by the passage of a well-organized primary vortex in the outer region. Further downstream, due to the growth in size of the secondary vortex and the mutual interaction between primary and secondary vortices, the primary vortex will be pushed into the outer low-speed region, while the secondary vortex is pulled up into the high-speed region. Thereafter, the secondary vortex will convect faster than the primary vortex and this will lead to the subsequent phenomenon of vortex lift-off from the wall surface. A very similar dynamic picture was independently obtained by Gogineni, Shih & Krothpalli (1993) using PIV measurements. In the light of this mechanism, Shih & Gogineni (1993) showed that by using a low-frequency high-amplitude external excitation, the jet can be deflected away from the wall and, consequently, the transitional process of the jet is accelerated.

In the above experiments, no supporting evidence was found with respect to the co-existence of the two instability modes, revealed theoretically by Chun & Schwarz (1967). Tsuji *et al.* (1977) associated the co-existence of the two instability modes with the two inflection points in the streamwise mean velocity profile, one in the outer region and the second on the wall. However, in their experiments, as was the

case in the previous experiments mentioned above, the existence of the second mode was not confirmed. Tsuji *et al.* attributed the absence of the second mode in their experiment to the fact that the velocity profiles did not sufficiently agree with the theoretical laminar profile found by Glauert. By calculating a pattern of streamlines of a disturbed motion, they were the first to associate the formation of the double row of vortices in the inner and outer layers with the linear stability theory. Using a curve fit to their experimental mean velocity profiles, the experimental amplification rates and distributions of the disturbance amplitude and phase compared well with the calculated results of the linear theory. The growth of a subharmonic wave in natural and forced wall jets, which was visualized by Bajura & Catalano (1975), was also evident from the hot-wire measurements of Tsuji *et al.* (1977).

Mele *et al.* (1986) demonstrated theoretically that the low-frequency mode (large-scale disturbances) is associated with the outer inflection point while the high-frequency mode (small-scale disturbances) is related to the mean velocity gradient in the vicinity of the wall. They showed that the unstable large-scale streamwise disturbances have the highest values in the outer region, while the highest values of the unstable small-scale disturbances are close to the wall. Hence, the outer inflection point renders the flow vulnerable to large-scale oscillations, while the effects of viscous instability seem to yield the amplification of the small-scale oscillations.

The possibility of the co-existence of the two instability modes was supported experimentally by Amitay (1994) and Cohen, Amitay & Bayly (1992). Furthermore, in order to control the relative dominance of each instability mode, Cohen *et al.* (1992) investigated theoretically the effects of subjecting the wall jet to small amounts of blowing or suction of fluid through the wall. They found a new family of laminar self-similar solutions in which the streamwise velocity U, and the normal velocity at the wall V_w, are given by

$$U(x,\eta) = (1-b)x^{1-2b}f'(\eta),$$

and

$$V_w(x) = -(1-b)f(0)x^{-b},$$

respectively, where the function f depends solely on the similarity variable, η, defined by

$$\eta = (1-b)y/x^b.$$

In the above expressions an arbitrary constant reference velocity scale, U_r, and a constant length scale, ν/U_r, were used to render all variables dimensionless; ν is the kinematic viscosity and x and y are the non-dimensional streamwise and transverse coordinates, respectively. The self-similar solutions differ from one another only in the power b. According to the values of b, or the more convenient parameter $\gamma = (2b-1)/(1-b)$, the family of self-similar solutions can be divided into three regimes: suction with $V_w < 0$ for $\gamma > 2$; Glauert solution with $V_w = 0$ for $\gamma = 2$; and blowing with $V_w > 0$ for $2 > \gamma > 1$.

These self-similar profiles were later confirmed experimentally by Amitay & Cohen (1993). By conducting temporal linear stability computations, using the above self-similar solutions as the unperturbed laminar flow, Cohen *et al.* (1992) showed that blowing stabilizes the inviscid mode while destabilizing the viscous one. The effect of suction was found to be just the opposite.

The purpose of the research presented here is to understand the interaction between the two different modes of instability supported by the wall jet. In the present work, which is the first stage of the study, we are mostly concerned with the linear phase

of the evolution of both modes. Using a small amount of surface velocity, it is demonstrated that the relative dominance of each one of the wall jet's modes can be controlled. We intend to use this method as a controlling tool in the next stage of the research wherein the coupling between the two modes will be investigated. Furthermore, it is hoped that by demonstrating experimental control over the relative dominance of each one of the wall jet's modes, other physical phenomena, wherein both types of instability co-exist simultaneously, will be better understood. One example is the inflection point in a distorted laminar boundary layer; another example is the separated boundary layer over a hump.

2. Experimental set-up

2.1. *The wall-jet apparatus*

The experiments were carried out in an open circuit air jet facility which consists of a 2 HP variable-speed centrifugal blower, a noise reduction chamber, a diffuser, and a settling chamber having one honeycomb and three screens followed by a contraction nozzle. The jet nozzle has an area contraction ratio of 30, and its shape fits a fifth-order polynomial profile. At the exit plane the height is 20 mm and the width is 600 mm. To improve the two-dimensionality of the incoming flow, a 20 mm by 600 mm metal strip was mounted spanwise at the downstream outer end of the nozzle along its top (that is, away from the wall). The strip was attached by a set of screws placed every 20 mm to provide a fine adjustment of the jet-exit height along the spanwise direction. The range of operating Reynolds number based on the jet-exit height and jet-exit velocity was between 125 and 466. The turbulence intensity at the nozzle-exit centre was less than 0.2%.

In order to control the amount of blowing or suction to which the wall jet was subjected, an apparatus consisting of a porous plate and a supporting box was built (figure 1*a*). According to previous theoretical results (Cohen *et al.* 1992), the required amount of injection (or suction) is a non-uniform function of the wall-jet streamwise direction. The box was therefore divided into two-dimensional cells. Each one could be subjected to a different and controlled pressured air flow or low vacuum for blowing or suction, respectively (see figure 1*b*). A detailed description of the apparatus and the method used to adjust the wall suction or blowing conditions, is given in Amitay (1994) and Amitay & Cohen (1993). It should be noted that measuring the normal velocity of the flow entering each cell is difficult because it is so low; in the sets of measurements reported here, the predicted normal velocity at the wall surface in the first cell is less than $2\,\mathrm{cm\,s^{-1}}$, two orders of magnitude smaller than the jet-exit velocity.

To observe the behaviour of small wavy disturbances under well-defined conditions, the wall-jet was artificially excited by vibrating a two-dimensional flap. The flap was placed 10 mm above the jet-exit upper side and extended 8 mm downstream of the jet-exit plane.

The measurements of the streamwise velocity were conducted using a standard Disa Model 55P11 single hot-wire probe with a 5 μm diameter tungsten sensor. The hot wire was kept at an overheat ratio of 1.6 and had a maximum frequency response of 30 KHz. It was calibrated in the exit plane of an axisymmetric jet, especially built for this purpose, against a standard Pitot tube used in conjunction with a MKS BARATRON model 398HD pressure transducer tube. Seven velocities were

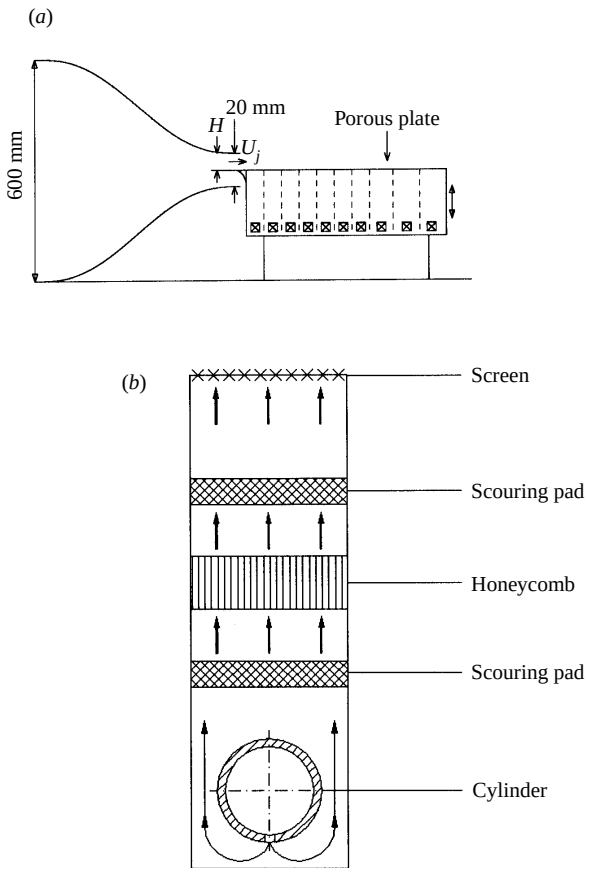

FIGURE 1. A schematic side-view of (*a*) the blowing and suction apparatus and of (*b*) one of its cells.

used for calibration. The raw data signals from the hot-wire anemometer and the BARATRON pressure transducer were acquired using a 486 PC.

The computer has eight differential channels of 12 bit Analog to Digital converters available for data acquisition with a maximum aggregate sample rate of 200 KHz. In addition, the computer is equipped with six channels of 12 bit Digital to Analog converters with a maximum aggregate output rate of 120 KHz. The D/A converters were used to generate sine wave forcing signals which were passed through an amplifier and then onto the mechanical vibrator which activated the two-dimensional flap. In addition, the computer controlled the positioning of the hot-wire probe via three stepper motors. The probe was mounted on a three-axis traversing mechanism which had a resolution of 5 μm in all three directions.

2.2. *Phase-locked data*

In order to retain phase information, the excitation signal was recorded in addition to the velocity signal. The hot-wire and function generator records, consisting of 256 points each, were digitized at a sampling frequency which was 35 times higher than the frequency of the excited wave, giving a cyclic resolution of 10° relative to the fundamental component of the phase-locked signal. To save time and computer memory, we distinguished between linear and nonlinear regions. In the linear region

the power spectrum of the ensemble-averaged velocity signals was almost identical to the averaged power spectra of all individual periods, and consequently the data acquisition procedure could be sped up. At each measuring point, 600 events were recorded and an ensemble average was formed. The fluctuating velocity was obtained by subtracting the local mean velocity from the ensemble signal, from which amplitude and phase of the disturbance were then obtained by using a direct Fourier transform. On the other hand, in the nonlinear region, the amplitude and phase of the disturbance were obtained for each period and were only then averaged. Unless noted otherwise, the level of forcing was defined as the maximum amplitude of the Fourier component, at the excitation frequency, of the streamwise velocity fluctuation normalized by the jet exit velocity and measured at 25 exit heights downstream of the exit plane.

3. Instability computations

To assess the effects of blowing or suction on the stability of the wall jet, the Orr–Sommerfeld equation for small wavy disturbances was solved numerically. This is a standard procedure, which was used by Cohen *et al.* (1992) for the temporal case. However, since we intend to compare the numerical calculations and the experimental results, the more appropriate spatial approach is used here to describe the growth of convective instabilities. As was shown by Gaster (1962) for small rates of amplification, and by Nayfeh & Padhye (1979) using the method of multiple scales, the spatial growth is related to the time growth by the group velocity.

The local linear stability analysis assumes that the mean flow can be considered locally parallel. This assumption is justified when the ratio between the transverse and the streamwise mean velocities is small. In the present case the ratio is proportional to the inverse of the local Reynolds number, R_δ^{-1}, where $R_\delta = U_m\delta/\nu \propto x^{1/(\gamma+2)}$, where U_m is the local maximum velocity and δ is the local thickness of the boundary layer, defined as the distance from the wall to the point where the velocity is one half the maximum in the outer region of the flow.

The effect of blowing and suction on the instability waves can be appreciated by considering the eigenvalues of the Orr–Sommerfeld equation corresponding to three values of γ. The exponential growth rates ($-\tilde{\alpha}_i$) and phase velocities ($\tilde{C}_{ph}$) of the waves calculated at a local Reynolds number of $R_\delta = U_m\delta/\nu = 150$ are plotted against their non-dimensional angular frequencies $\tilde{\beta}$ in figures 2(*a*) and 2(*b*) respectively. The relevant scales U_m and δ are used to render all variables dimensionless. Three cases, representing the suction ($\gamma = 3$), Glauert ($\gamma = 2$) and blowing ($\gamma = 1.5$) solutions, are shown. Blowing tends to destabilize the small-scale (high-$\tilde{\beta}$) disturbances but stabilizes the larger scales (small $\tilde{\beta}$) while suction does the opposite. Similar results calculated at a local Reynolds number of 800 are presented in figure 3. At this relatively high local Reynolds number, the instability mode is clearly separated into two modes having two different dispersion relations. Blowing tends to destabilize the small-scale (high-frequency) disturbances but stabilizes the larger scales. The effect of suction is just the opposite.

The neutral stability curves ($\tilde{\alpha}_i = 0$), corresponding to these three wall conditions, are shown in figure 4(*a*), where $\tilde{\beta}$ is plotted versus R_δ. For each case, three regions of instability can be distinguished: region I where only a single mode is unstable; region II where two unstable modes correspond to two different bands of frequencies and region III where two bands of unstable modes have an overlapping region in which two waves have the same frequency, but different eigenvalues. These regions are indicated in figure 4(*a*) only for the Glauert case. Representative amplification

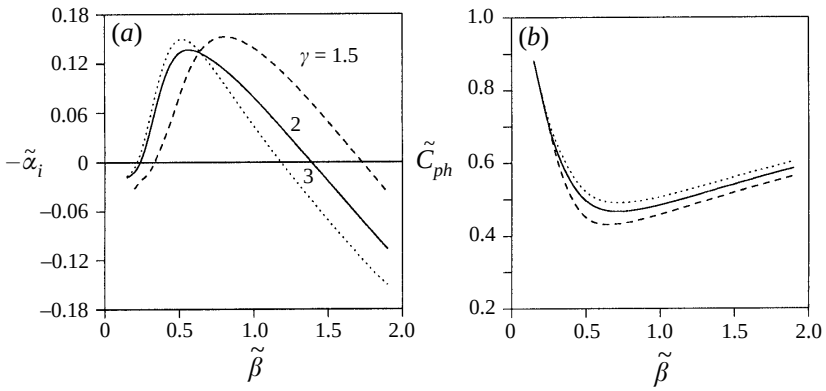

FIGURE 2. (*a*) Spatial amplification rate $\tilde{\alpha}_i$ and (*b*) phase velocity $\tilde{C}_{ph}$ versus non-dimensional frequency $\tilde{\beta}$ at $R_\delta = 150$ and for $\gamma = 1.5$ (blowing), $\gamma = 2$ (Glauert) and $\gamma = 3$ (suction).

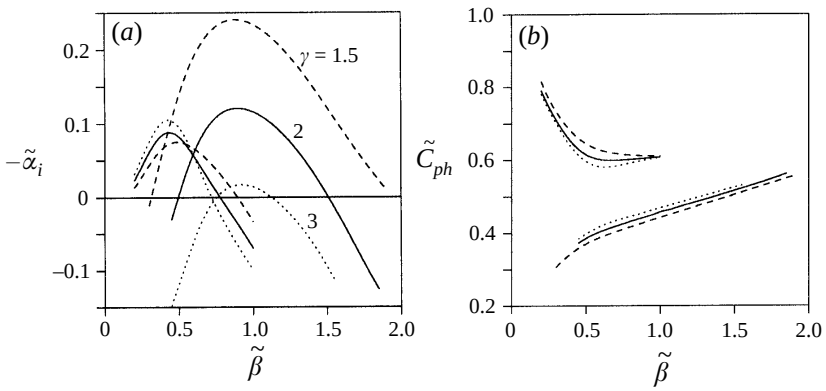

FIGURE 3. As figure 2 but at $R_\delta = 800$.

curves corresponding to each of the instability regions are shown in figures 4(*b–d*), for $\gamma = 2$.

As can be seen, when blowing or suction are applied, region III begins at a lower or a higher local Reynolds number, respectively. Furthermore, the instability regions above and below (with respect to frequency) region III are increased and decreased, respectively, when blowing is applied. The effect of suction is just the opposite. This is related to the fact that blowing tends to destabilize the high-frequency waves and to stabilize the lower-frequency ones.

4. Comparison between theory and experiments

Although a detailed comparison between the self-similar mean flow solutions and measurements has already been presented by Amitay & Cohen (1993), we include here one example thereof which is relevant in explaining some of the issues discussed in the following sections. Throughout the mean flow experiments, five different values of γ were used, corresponding to two levels of wall blowing with $\gamma = 1.5$ and 1.7, two levels of wall suction with $\gamma = 2.3$ and 3, and the case in which no blowing or suction was applied ($\gamma = 2$). A right-handed coordinate system is defined with $\hat{X}$, $\hat{Y}$, $\hat{Z}$ as the downstream, wall-normal and spanwise (parallel to the wall) directions, respectively,

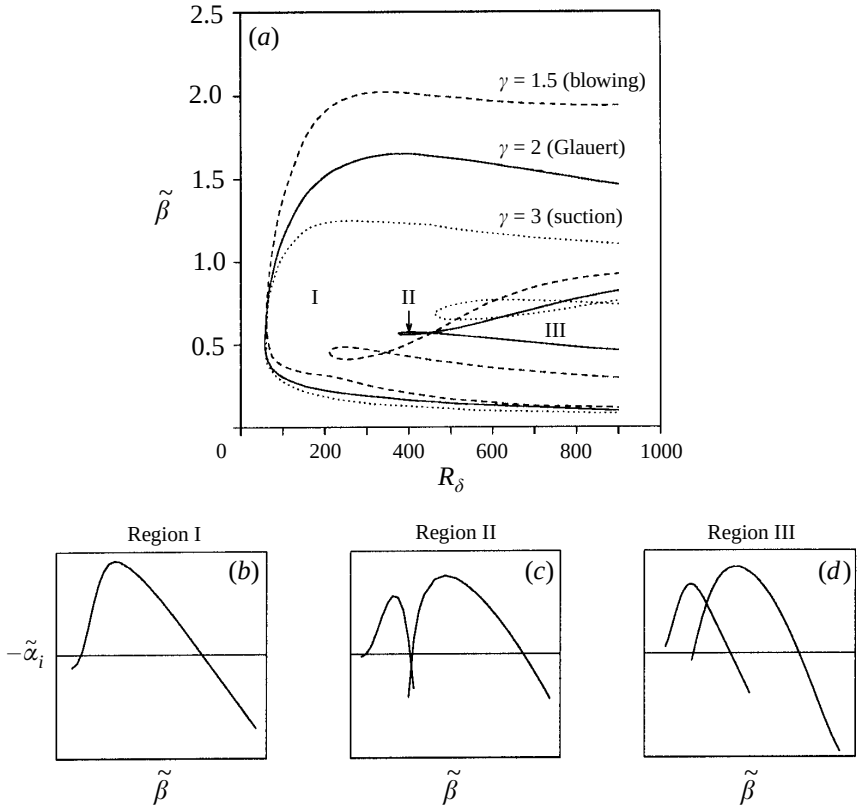

FIGURE 4. (*a*) Neutral stability curves for $\gamma = 1.5$, 2 and 3; (*b*), (*c*) and (*d*) representative amplification curves for regions I, II and III, respectively.

with $\hat{U}$, $\hat{V}$ and $\hat{W}$ being the corresponding velocity components. All quantities with carets are dimensional.

The mean profiles of the streamwise velocity measured when the jet-exit Reynolds number was $R_j = 466$, based on the jet-exit velocity $U_j = 7\,\mathrm{m\,sec^{-1}}$ and jet-exit width $H = 1.0\,\mathrm{mm}$, are plotted in dimensional coordinates in figure 5. The full profiles at $\hat{X}/H = 30$ are displayed in figure 5(*a*), while the corresponding inner layers are shown in greater detail in figure 5(*b*). The various symbols represent the measurements obtained at different wall conditions and the solid lines are the corresponding theoretical solutions.

The downstream development of the local maximum velocities and the local boundary layer thicknesses at $R_j = 466$ are shown in figures 6(*a*) and 6(*b*), respectively. The small vertical arrows in figure 6(*a*) indicate the last streamwise locations where the measured profiles conformed to the laminar solutions. The agreement between the measurements and the theoretical solutions is very good, indicating that the correct streamwise distributions of the normal velocity at the wall were obtained. Accordingly, the ratio between the wall-normal velocity and the jet-exit velocity at the jet-exit plane is approximately 0.25% for blowing with $\gamma = 1.5$ and -0.27% for suction with $\gamma = 3$. As is evident from the self-similar solution, this ratio decreases with downstream distance as $(\hat{X} - \hat{X}_0)^{-(\gamma+1)/(\gamma+2)}$, where $\hat{X}_0$ is a constant shift in the streamwise direction (virtual origin).

Similar results (see Amitay 1994 and Amitay & Cohen 1993) for $R_j = 180$ and 270

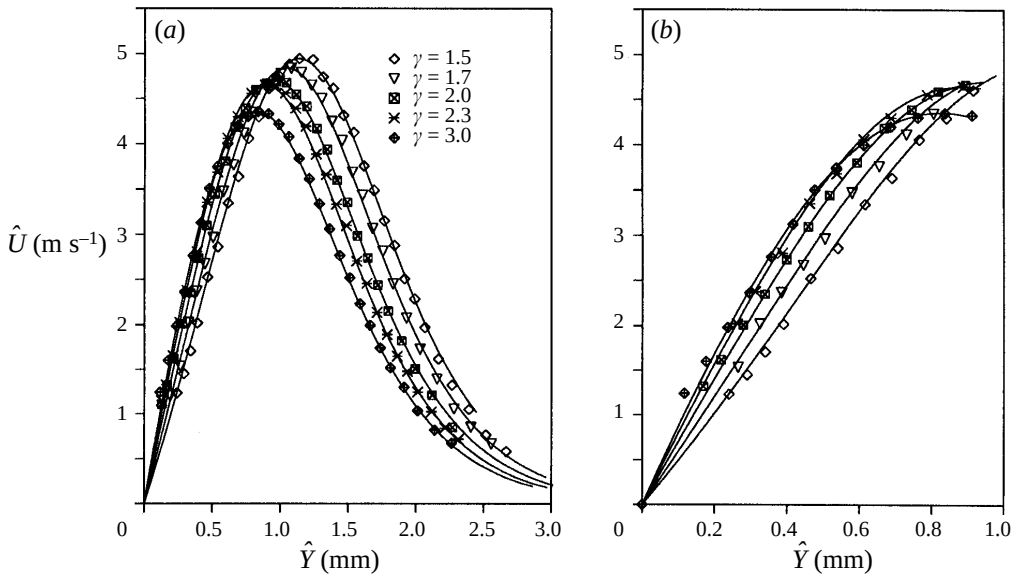

FIGURE 5. (*a*) Comparison between the theoretical (solid lines) and measured streamwise mean velocity profiles (symbols) for various values of γ at $\hat{X}/H = 30$ and $R_j = 466$. (*b*) The corresponding inner regions.

indicate that the non-dimensional downstream distances $\hat{X}/H$ where the measured profiles conformed to the theoretical ones, are increased as the jet-exit Reynolds number is decreased.

4.1. *Instabilities in natural wall jet*

In order to examine the effects of blowing and suction on the evolution of instabilities in natural wall jets, experimental power spectra corresponding to wall conditions of $\gamma = 3$, 2 and 1.7, are examined in relation to the trends predicted by the linear stability theory. The spectral distributions correspond to measurements obtained in the inner and the outer regions of the boundary layer, where the mean velocity equals 0.55 ($\hat{Y}_{55}$) and 0.80 ($\hat{Y}_{80}$) of the maximum velocity, respectively, and at several streamwise positions between $\hat{X}/H = 25$ to 60. The jet-exit velocity and width were $U_j = 7\,\mathrm{m\,s^{-1}}$ and $H = 1\,\mathrm{mm}$, respectively, which resulted in a jet-exit Reynolds number of 466. For the Glauert case, the local Reynolds numbers were approximately 500 and 580 at the first and last streamwise locations, respectively. When blowing and suction were applied, the corresponding local Reynolds numbers were 570 to 650 and 430 to 490, respectively.

The disturbances' exponential growth rates for $\gamma = 3$, 2 and 1.7 are plotted against their non-dimensional frequencies in figure 7. For the case of $\gamma = 2$ the calculations were carried out at two local Reynolds numbers of 500 and 580, corresponding approximately to the lower and upper limits of the experimental values. There is a slight difference between the eigenvalue distributions associated with the two Reynolds numbers. Thus, in conjunction with the qualitative comparison between the experimental results and the local stability calculations, the effect of the streamwise variation of the local Reynolds number is secondary. The Reynolds number used in the calculations of the eigenvalues for $\gamma = 3$ and 1.7 was chosen to be between the two local Reynolds numbers measured at the first and last streamwise locations.

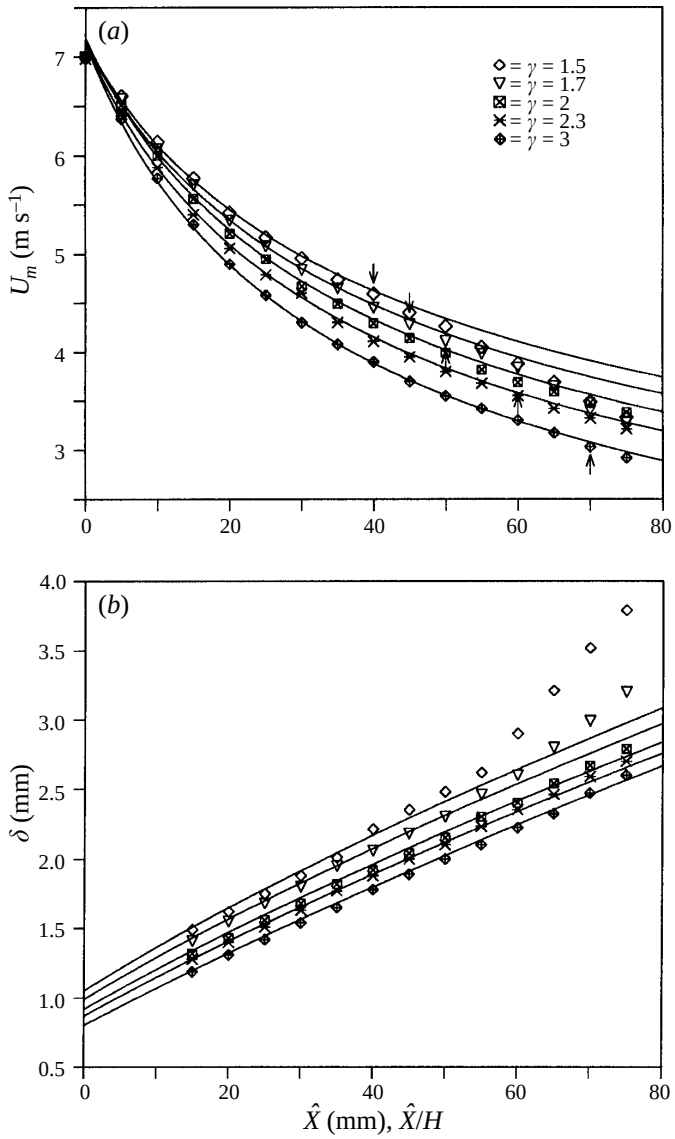

FIGURE 6. The streamwise variation of (*a*) the local maximum velocity U_m and (*b*) the local boundary layer thickness δ, at $R_j = 466$ for various values of γ. The solid lines represent the laminar solutions.

Accordingly, the corresponding local Reynolds numbers for $\gamma = 3$ and 1.7 are $R_\delta = 450$ and 600, respectively.

The spectral distributions measured at two streamwise locations and at two distances from the wall where $\hat{Y} = \hat{Y}_{55}$ and $\hat{Y} = \hat{Y}_{80}$ are shown in figure 8 for the three wall conditions mentioned above. The first streamwise position for all cases presented in figure 8 is $\hat{X}/H = 25$, while the further downstream positions corresponding to $\gamma = 3$, 2 and 1.7 are $\hat{X}/H = 60$, 40 and 40, respectively. This choice of the second streamwise position is due to the difference in the spectral spatial evolution associated with the three wall conditions.

In the following, we attempt to relate qualitatively the spectral measurements

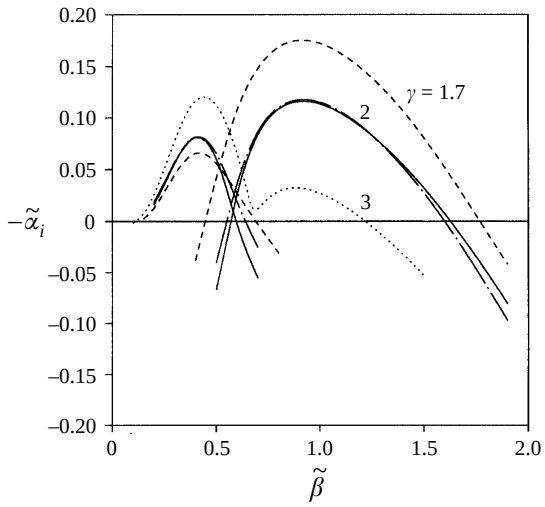

FIGURE 7. Spatial amplification rate $\tilde{\alpha}_i$ versus non-dimensional frequency $\tilde{\beta}$ at $R_\delta = 450$ (dotted lines), 500 (solid lines), 580 (dashed-dotted lines) and 650 (dashed lines) for $\gamma = 3$, 2, 2 and 1.7, respectively.

presented in figure 8 to the amplification curves shown in figure 7. It is not intended to quantitatively validate experimentally the theoretical predictions but rather to show the consistency between the two. It should be noted that although for the Glauert and suction cases a clear distinction between the inviscid and viscous modes was better observed at a higher jet-exit Reynolds number, these results are not presented here since the mean flow under these conditions did not conform to the laminar solution when blowing ($\gamma = 1.7$) was applied. In all cases shown in figure 8, the magnitude of the spectra at $\hat{Y}_{55}$ is higher than that obtained at $\hat{Y}_{80}$ for the range of $\tilde{\beta} = 2\pi f\delta/U_m$ approximately between 0.8 and 2.2, where f is the dimensional frequency. For lower frequencies ($0 < \tilde{\beta} < 0.4$) the magnitude of the spectra at $\hat{Y}_{55}$ is lower than that obtained at $\hat{Y}_{80}$. This trend is consistent with the prediction of the linear stability theory (see figure 9 below and Cohen *et al.* 1992), according to which the high-frequency viscous mode (in the range of $\tilde{\beta}$ approximately between 0.8 and 2.2) dominates the inner region, while the low-frequency inviscid mode prevails in the outer region.

By comparing figures 8(*a*) and 8(*e*), it is evident that the bandwidth of frequencies associated with the viscous mode is wider for blowing and narrower for suction, a trend anticipated from the corresponding exponential growth rates shown in figure 7. Moreover, in accordance with the theoretical results presented in figure 7, the initial growth of the high-frequency viscous mode is higher when blowing is applied and lower when suction is applied. Experimentally, this can be deduced by comparing the power of the corresponding spectral distributions at the first streamwise position shown in figures 8(*a*) and 8(*e*) (assuming that their initial spectra are almost identical), or by comparing power spectra growth between the first and second streamwise locations for both modes (figures 8*a*, *b* and 8*e*, *f*, respectively). Finally, the most energetic waves are associated with the low-frequency inviscid mode when suction is applied, and with the high-frequency viscous mode when blowing is applied.

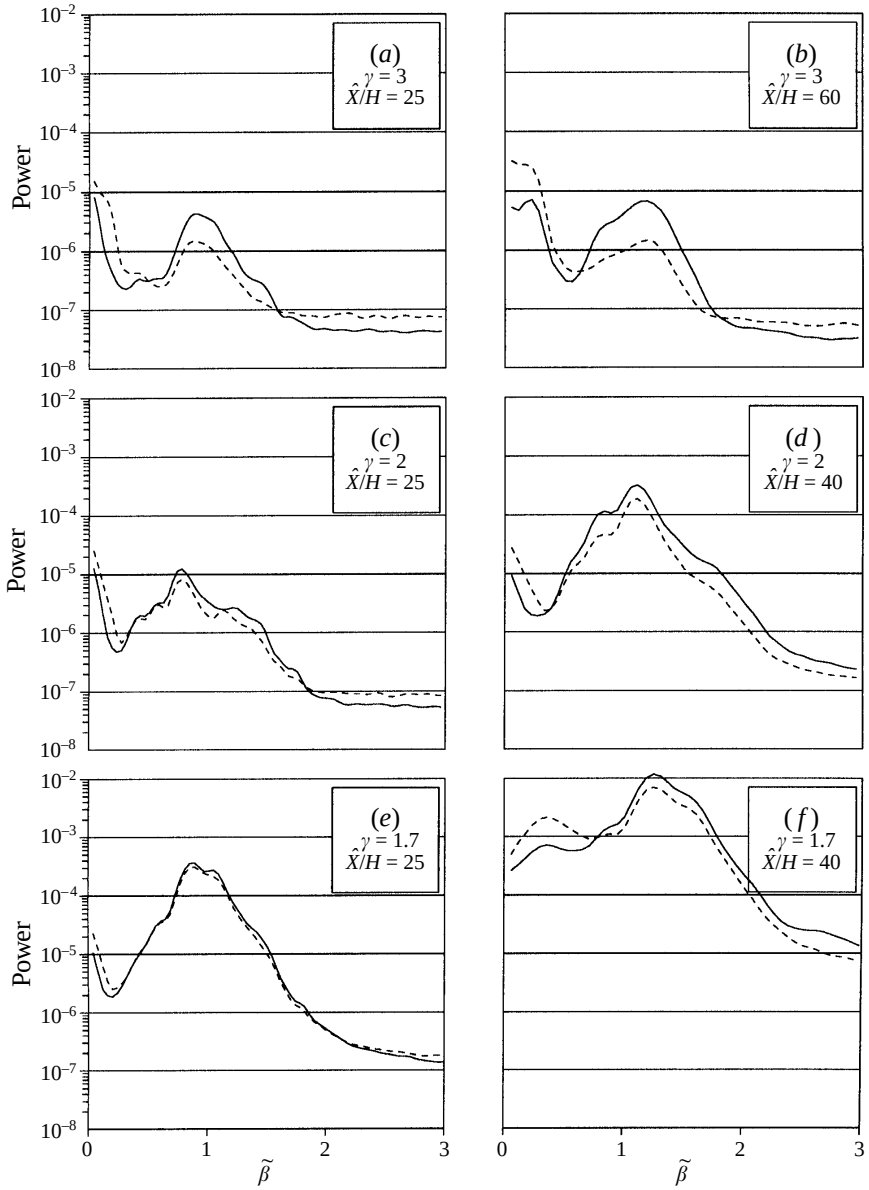

FIGURE 8. Power-spectrum distributions of the streamwise velocity versus $\tilde{\beta} = 2\pi f\delta/U_m$, measured at several downstream distances at $R_j = 466$ and at $\hat{Y} = \hat{Y}_{55}$ (inner region, solid lines) and $\hat{Y} = \hat{Y}_{80}$ (outer region, dashed lines), for $\gamma = 3$, 2 and 1.7. The local Reynolds numbers are: (*a*) 434, (*b*) 488, (*c*) 515, (*d*) 549, (*e*) 569 and (*f*) 611.

4.2. *Comparison of the forced wall-jet data with linear stability analysis*

In this subsection, the structure and evolution of two-dimensional streamwise disturbances are studied under controlled conditions. Different disturbances were introduced into the flow by vibrating a two-dimensional flap at various frequencies and amplitudes. Phase-locked data were measured, analysed and compared with the theoretical predictions of the linear stability theory.

First, the spanwise uniformity of the fundamental component of the excited wave,

when the jet was subjected to three wall conditions ($\gamma = 2, 3$ and 1.7), was characterized by applying a two-dimensional Fourier transform to phase-locked velocity signals measured at several downstream positions and at 1 mm intervals over a span of 60 mm. It was found (see Amitay 1994) that the two-dimensionality of the fundamental component prevails throughout the boundary layer. Therefore, the development of the fundamental component in the following subsections will be analysed based upon phase-locked data measured along the centreline.

4.2.1. *The effect of blowing and suction on the cross-stream distribution of the streamwise disturbance*

The normalized modulus of the fluctuating streamwise velocity $|\tilde{u}|$ at a local Reynolds number of $R_\delta = 469$ and for three values of γ corresponding to Glauert ($\gamma = 2$), suction ($\gamma = 3$) and blowing ($\gamma = 1.5$), are plotted in figure 9. For large-scale inviscid disturbances ($\tilde{\beta} = 0.431$) the maximum of the amplitude distribution is in the outer region (figure 9*a*), while for small-scale viscous disturbances ($\tilde{\beta} = 0.972$) the maximum is close to the wall (figure 9*b*). The amplitudes were normalized by the values of the outer and inner maxima in figures 9(*a*) and 9(*b*), respectively. The non-dimensional frequencies of the excited waves were chosen to correspond approximately to maximum growth of the waves above and below region III (the region in which two amplified waves co-exist simultaneously, see figure 4). Thus, for each of the forced waves, only a single mode could be amplified, according to linear stability theory. The lines are the theoretical eigenfunctions for $\gamma = 1.5$, 2 and 3 while the symbols are the corresponding phase-locked results when the wall jet was subjected to two-dimensional excitations. In all cases, the agreement between the theory and the experiments is fairly good, except for two regions: the outer region wherein the streamwise mean velocity is less than 10% of the local maximum velocity, and the valley between the two main maxima of the eigenfunction, the height of which is overpredicted by the theory.

The above results suggest that the small-scale disturbances are associated with the viscous shear layer mode, while the large-scale ones are associated with the outer inviscid instability. These results are in agreement with previous calculations done by Mele *et al.* (1986) for a plane wall jet where neither suction nor blowing were applied. As is predicted by the theory and confirmed experimentally, blowing and suction tend to increase and decrease, respectively, the ratio between the outer and inner amplitude maxima for both the high- and low-frequency modes. This is related to the increase and decrease of the slope of the mean velocity profile at the wall when suction and blowing are applied (see figure 5). It should be noted that the experimental results for the three cases presented here were obtained at different jet-exit conditions so that the local Reynolds number and the non-dimensional frequency at $\hat{X}/H = 30$ were the same.

In order to characterize the stability of the wall jet, the streamwise evolution of the disturbances in the following four regions were examined (see figure 4): region I, above region III, across region III and across region II .

4.2.2. *Region I*

In region I only a single mode exists. The measured cross-stream distributions of the fundamental component of the streamwise velocity fluctuations at three downstream locations where $\hat{X}/H = 50$, 70 and 90, are shown in figures 10(*a*), 10(*b*) and 10(*c*) and compared with theoretical computations for $\gamma = 2$, 3 and 1.7, respectively. The symbols represent the measured phase-locked data, while the solid lines are the

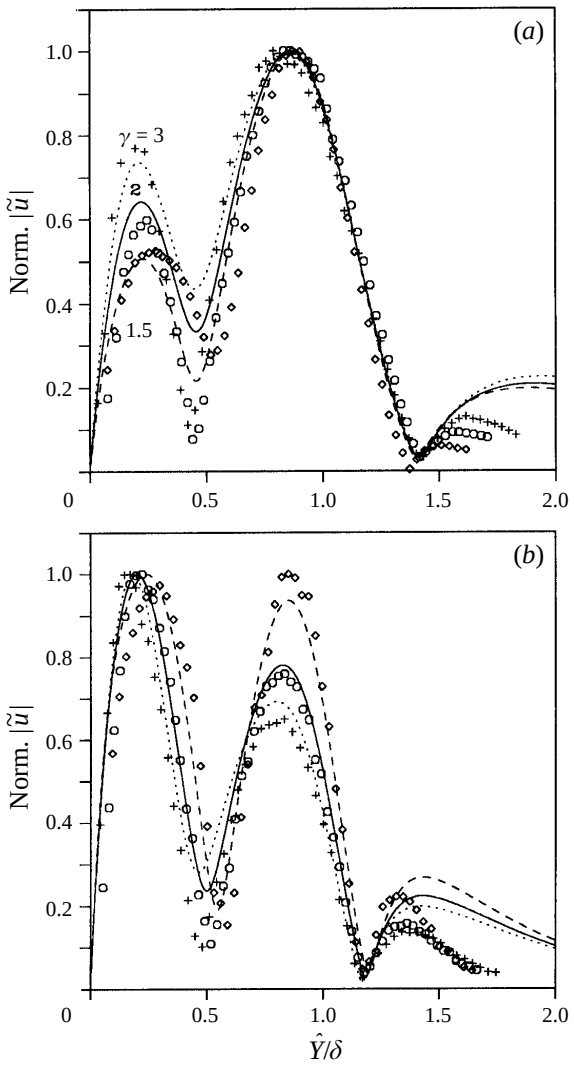

FIGURE 9. The normalized modulus $|\tilde{u}|$ at $\hat{X}/H = 30$, $R_\delta = 469$. (*a*) $\tilde{\beta} = 0.431$ and (*b*) $\tilde{\beta} = 0.972$. The symbols represent the experimental data while the lines are the corresponding theoretical solutions: – – –, ◇, $\gamma = 1.5$, ——, ○, $\gamma = 2$; · · · · · ·, +, $\gamma = 3$.

corresponding theoretical results. For all cases the jet-exit velocity was $U_j = 2.5\,\mathrm{m\,s^{-1}}$, the jet-exit height was $H = 0.75\,\mathrm{mm}$, the forcing frequency was $f_{ex} = 40\,\mathrm{Hz}$ and the maximum amplitude of the streamwise disturbance at $\hat{X}/H = 30$ was 0.16% of the jet-exit velocity. Under these experimental conditions, the non-dimensional forcing frequency throughout the entire measured downstream domain corresponded to region I. Although the experimental conditions were the same for all cases, the non-dimensional local frequency when suction was applied was higher than the corresponding frequency when no blowing or suction were applied, whereas the value of the local Reynolds number was lower. When blowing was applied, these trends were just the opposite.

The experimental data follow the trends predicted by the linear stability theory, according to which the ratio between the inner and outer maxima of the streamwise

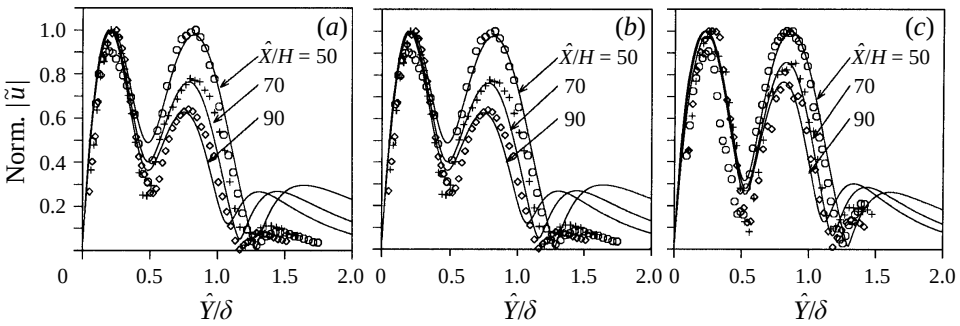

FIGURE 10. Comparison between the measured (symbols: ○, $\hat{X}/H = 50$; +, 70; ◇, 90) and theoretical (lines) cross-stream distributions of $|\tilde{u}|$ at three downstream locations and at $R_j = 125$. (*a*) $\gamma = 2$, (*b*) $\gamma = 3$ and (*c*) $\gamma = 1.7$.

eigenfunctions increases with downstream distance, while the ratio between the width of the disturbed region and the local boundary layer thickness decreases. These are not surprising results since as the downstream distance increases, so does the non-dimensional frequency $\tilde{\beta}$ and consequently smaller scales, governed by the near-wall region, become more dominant.

In order to compare the measured streamwise amplification of the disturbance with the theoretical prediction, the method of multiple scales to account for the mean flow divergence and to describe the growth of a two-dimensional wave disturbance in boundary layers was applied to wall-jet flows. In this approach (see for example Bouthier 1973; Gaster 1974; Saric & Nayfeh 1975) one uses the amplitude distributions of the parallel theory as a first approximation for an extension of the theory to include non-parallel effects. The results of the direct numerical simulation carried out by Fazel & Konzelmann (1990) clearly show that the application of this approach to a laminar boundary layer is well justified.

In the comparisons described below, the multiple scales procedure, used successfully by Cohen (1994) to describe the initial growth of a wave packet in a laminar boundary layer, is applied to wall-jet flows. However, unlike the case of conventional boundary layer flows in which the second-order boundary layer corrections of the mean flow can be neglected, in wall-jet flows these corrections are of the same order of magnitude as the other terms associated with the divergence of the mean flow and therefore must be included in the analysis. In the Appendix the second-order correction to the Glauert wall-jet solution found by Plotkin (1970) is generalized to include the cases when the wall jet is subjected to wall blowing and suction.

The streamwise growth of the disturbance measured at two vertical locations $\hat{Y} = \hat{Y}_{55}$ and $\hat{Y} = \hat{Y}_{80}$ is shown for $\gamma = 2$ (11*a*), $\gamma = 3$ (11*b*) and $\gamma = 1.7$ (11*c*). The lines are the corresponding predictions of the linear stability theory at $\hat{Y}_{55}$ and $\hat{Y}_{80}$. The amplitudes were normalized with respect to their values at the first measured $\hat{X}$ location. For each value of γ the amplification of the disturbance in the inner region is greater than that in the outer region. This is directly related to the ratio between the inner and outer maxima of the eigenfunction, which as mentioned above increases with downstream distance. The agreement between the theoretical predictions and the experiments in all cases is good. As predicted by the theoretical amplification curves (see also figure 2) and confirmed experimentally, the initial amplification of the disturbance when suction or blowing are applied is larger or smaller, respectively,

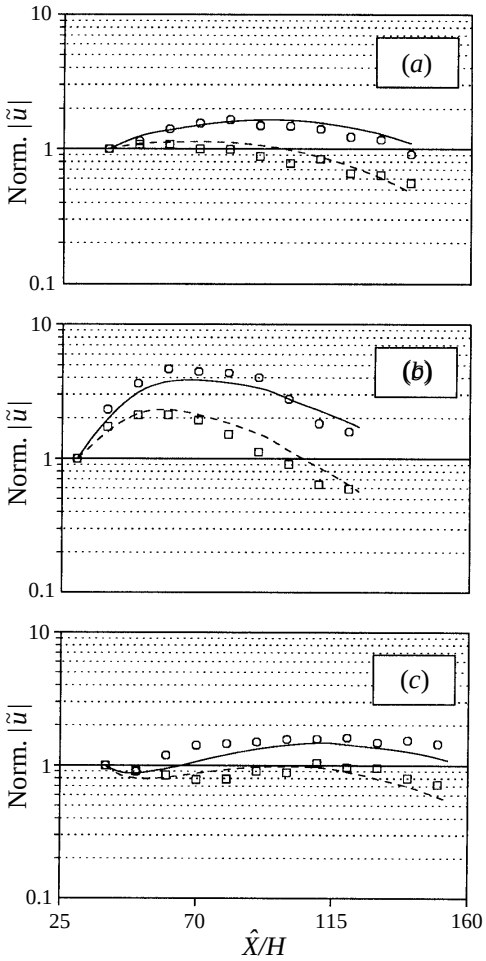

FIGURE 11. Comparison between the measured (symbols) and theoretical downstream development of $|\tilde{u}|$ measured at $R_j = 125$ and $\hat{Y} = \hat{Y}_{55}$ (solid lines, ○) and at $\hat{Y} = \hat{Y}_{80}$ (dashed lines, □). (*a*) $\gamma = 2$, (*b*) $\gamma = 3$ and (*c*) $\gamma = 1.7$.

than that corresponding to $\gamma = 2$, whereas the opposite trend is observed at distances further downstream.

4.2.3. *Above region III*

In the domain above region III (with respect to figure 4) the viscous mode is the prevailing one. To follow the evolution of this mode experimentally, the following set of parameters was used: the jet-exit velocity was $2.9\,\mathrm{m\,s^{-1}}$, the jet-exit height 2.4 mm, the forcing frequency 80 Hz and the maximum amplitude of the streamwise disturbance at $\hat{X}/H = 25$ was 0.16% of the jet-exit velocity. The cross-stream distributions of the streamwise velocity fluctuations at three downstream locations ($\hat{X}/H = 25, 50$ and 60) are shown in figures 12(*a*) and 12(*b*) for $\gamma = 2$ and 3, respectively. The agreement between the theoretical results (solid lines) and the experiments (symbols) is good. The streamwise eigenfunctions follow the same trend as in region I: the ratio between their inner and outer maxima increases with downstream distance, while the ratio between the width of the disturbed region and

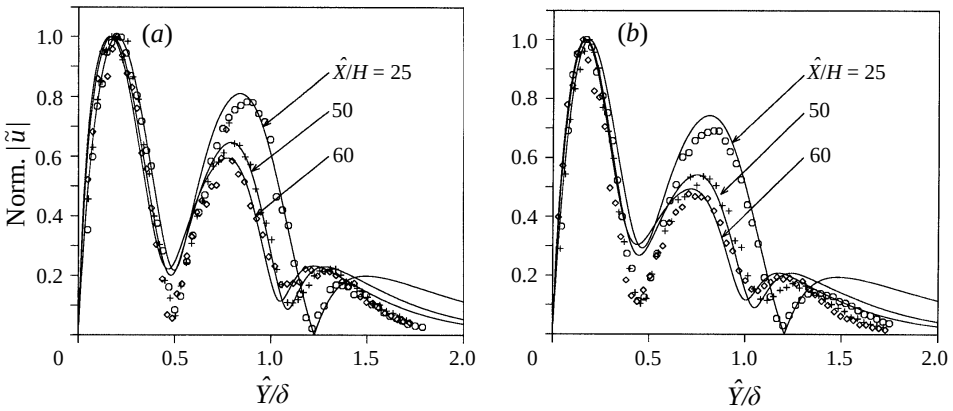

FIGURE 12. Comparison between the measured (symbols) and theoretical (lines) cross-stream distributions of $|\tilde{u}|$ at three downstream locations and at $R_j = 466$. (*a*) $\gamma = 2$ and (*b*) $\gamma = 3$.

the local boundary layer thickness decreases. Similar results were obtained (but are not shown here) for the case in which blowing was applied. For this case the distance upstream of which the mean flow conformed to the laminar solution was relatively shorter, $\hat{X}/H \approx 40$ and 45 for $\gamma = 1.5$ and 1.7, respectively (see figure 6).

The downstream developments of the streamwise disturbance for four values of $\gamma = 1.5, 1.7, 2$ and 3, measured at $\hat{Y} = \hat{Y}_{80}$ are shown in figure 13. Except for the case in which $\gamma = 1.5$, the symbols represent measurements obtained when the disturbance level at $\hat{X}/H = 25$ was $|\tilde{u}|_{max}/U_j = 0.16\%$, 0.27% and 0.37%, respectively, while the dashed lines are the normalized theoretical predictions. For the case in which a high level of blowing was used ($\gamma = 1.5$), the power of spectral distribution of the unforced flow was relatively very high. Therefore higher levels of excitations were used and consequently the initial disturbance levels as measured at $\hat{X}/H = 25$ were 1.67%, 2.27% and 3.1%, respectively.

For the Glauert and the suction cases the experimental amplitudes follow the theoretical amplification curves, although the experimental amplitudes are slightly greater than the predictions of the linear theory. Furthermore, throughout the downstream domain for the suction and Glauert cases the three sets of the experimental results, corresponding to the three levels of excitation used, collapse on a single curve indicating that nonlinear effects are negligible. When blowing was applied, the measured amplitudes were higher than or equal to the theoretical predictions only for a short streamwise distance (where nonlinear effects were still insignificant), beyond which a sharp decrease in their values was observed. This behaviour is related to the laminar-to-turbulent transition location of the natural wall jet. As mentioned before in relation to figure 6, the transition begins at $\hat{X}/H \approx 40$ and 45 for $\gamma = 1.5$ and 1.7, respectively. These positions correlate well with the corresponding locations where the amplitudes of the forced waves begin to depart sharply from the theoretical amplification curves.

4.2.4. *Across region III*

In region III the inviscid and viscous modes co-exist simultaneously, i.e. both modes have the same frequency but different eigenvalues and eigenfunctions. Thus, the fundamental component of the measured phase-locked data contains a combination of both modes. In order to decompose the experimental signals according to their respective contributions, we followed the method proposed by Tumin *et al.* (1996),

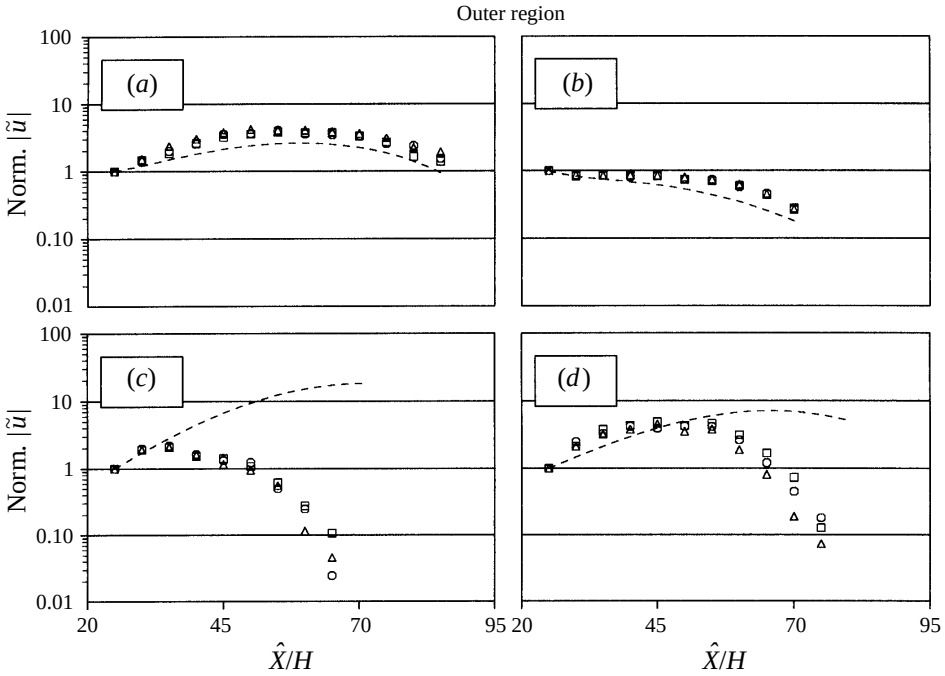

FIGURE 13. Comparison between the measured (symbols) and theoretical (dashed lines) downstream development of $|\tilde{u}|$ measured at $R_j = 466$ and $\hat{Y} = \hat{Y}_{80}$. (*a*) $\gamma = 2$, (*b*) $\gamma = 3$ (*c*) $\gamma = 1.5$ and (*d*) $\gamma = 1.7$. For cases (*a*), (*b*) and (*d*) the squares, circles and triangles represent measurements obtained when the disturbance level at $\hat{X}/H = 25$ was $|\tilde{u}|_{max}/U_j = 0.16\%$, 0.27% and 0.37%, respectively, while for case (*c*) the corresponding disturbance levels were 1.67%, 2.27% and 3.1%, respectively.

who applied the bi-orthogonal eigenfunction system, formulated by Zhigulev & Tumin (1987) to analyse such cases in transitional boundary layers and wall jets.

To follow the evolution of both modes across region III, the following set of experimental parameters was used: the jet-exit velocity was $7\,\mathrm{m\,s^{-1}}$, the jet-exit height 1 mm, the forcing frequency 180 Hz and the maximum amplitude of the streamwise disturbance at $\hat{X}/H = 25$ was 0.16% of the jet-exit velocity. Under these experimental conditions the non-dimensional forcing frequency for $\gamma = 2$ corresponded to the region below region III at the first downstream station. Three cases, representing suction ($\gamma = 3$), Glauert ($\gamma = 2$) and blowing ($\gamma = 1.7$), were measured. Although the experimental conditions were the same for all three cases, the local Reynolds numbers obtained for the suction and blowing cases were lower and higher, respectively, than that of the Glauert one. Moreover, since for $\gamma = 3$ the Reynolds number indicating the beginning of region III shifted towards a higher value (see figure 4), the corresponding domain of $\tilde{\beta}$ versus R_δ was within region I and therefore will not be presented here. On the other hand, the effect of blowing was to shift the first measured downstream position to a point within region III.

The measured amplitude and phase distributions of the streamwise velocity fluctuations at three downstream locations for $\gamma = 2$ are shown in figure 14(*a–f*) and compared with theoretical computations of the viscous and inviscid modes. As can be seen, the experimental data do not fit either of them. However, the experimental amplitude and phase distributions agree well with the corresponding theoretical distributions (solid lines) based on the weighted contributions of both modes as obtained

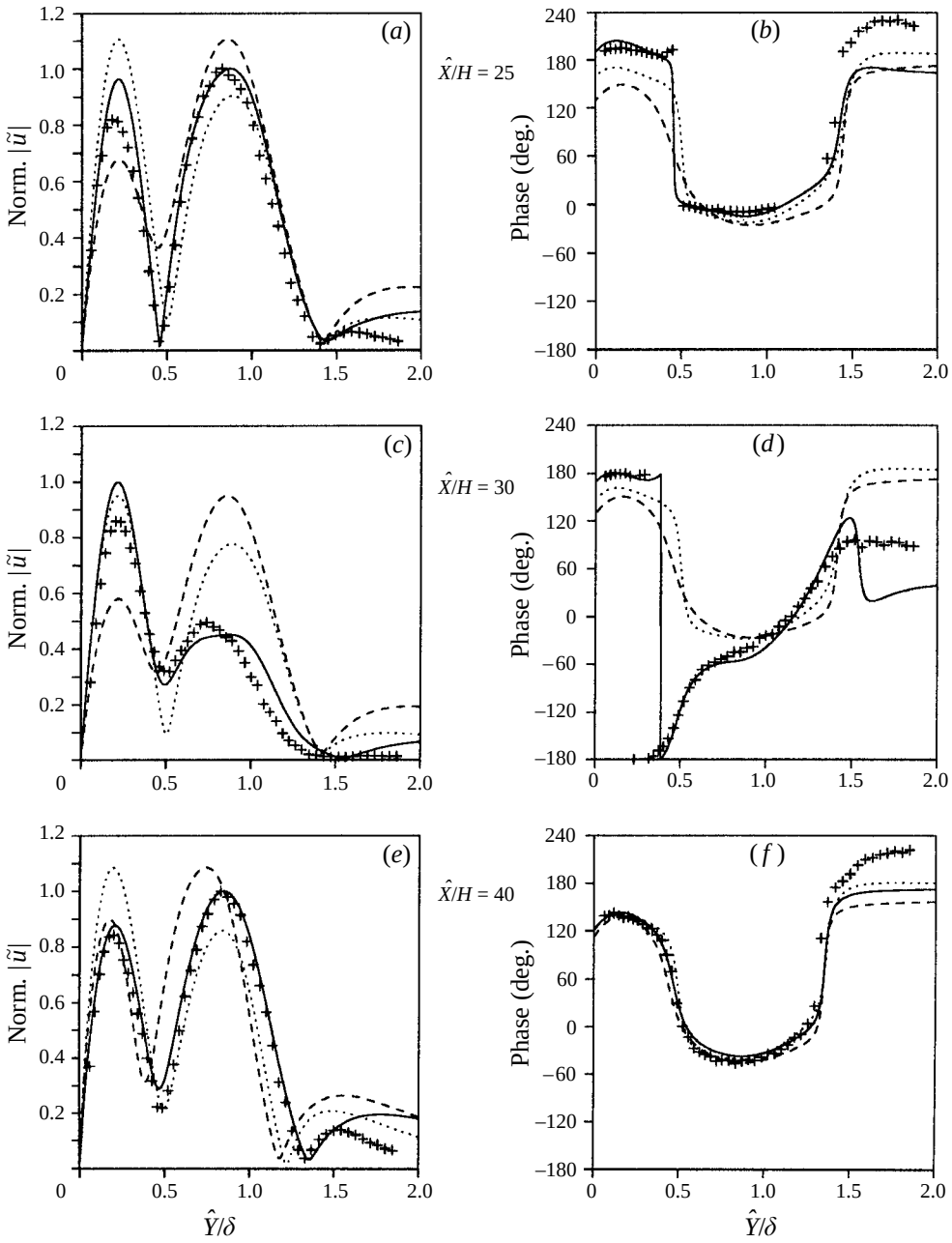

FIGURE 14. The amplitude and phase cross-stream distributions of $\tilde{u}$ at $R_j = 466$, $\gamma = 2$ and three downstream locations. The symbols correspond to the experimental data, the dotted lines to the theoretical distributions of the viscous mode, the dashed lines to the theoretical distributions of the inviscid mode and the solid lines to the theoretical distributions based on the weighted contributions of both modes.

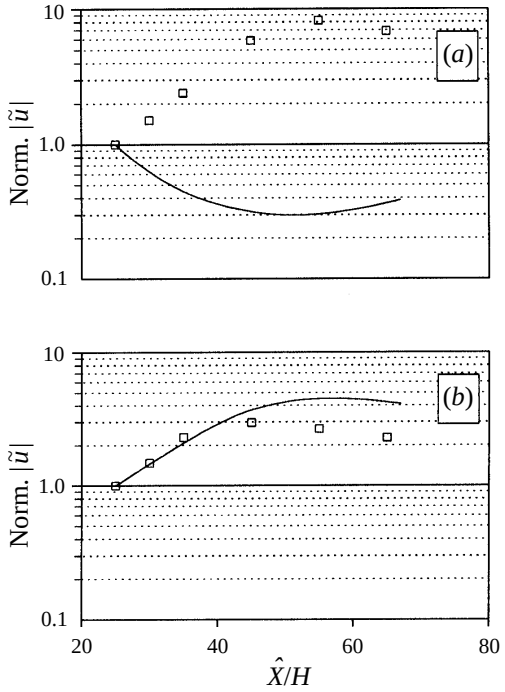

FIGURE 15. Comparison between the measured (symbols) and theoretical (solid lines) downstream development of (*a*) the viscous mode and (*b*) the inviscid mode of $|\tilde{u}|$ measured at $R_j = 466$, $\gamma = 2$ and $\hat{Y} = \hat{Y}_{55}$.

using the above mentioned decomposition method (Tumin *et al.* 1996). The maximum values of the latter were used to normalize all of the theoretical and experimental distributions.

After decomposing the experimental signals, the downstream development of each mode measured at $\hat{Y} = \hat{Y}_{55}$ was found and compared to the theoretical prediction. This downstream development is shown in figures 15(*a*) and 15(*b*) for the viscous and inviscid modes, respectively. While the measured amplitude of the inviscid mode follows the theoretical amplification curve quite accurately, there is a severe difference between the experimental data and the theoretical prediction with respect to the viscous mode. In fact, the two show opposite trends.

A typical decomposition of the two modes, obtained when wall blowing ($\gamma = 1.7$) was applied, is presented in figure 16 which follows the same structure as in figure 14. As in the case of $\gamma = 2$, the experimental amplitude and phase distributions do not fit either of the two theoretical modes, while they are fairly well described by the linear stability theory when the orthogonalization decomposition method is used.

4.2.5. *Across region II*

In this subsection, the evolution of the excited wavy disturbances across region II (see figure 4) is briefly discussed. According to the linear stability theory, below region II (low frequencies) only the inviscid mode is unstable. In region II itself both modes are stable, whereas above region II (high frequencies) only the viscous mode should be amplified. However, when following the evolution of an excited instability wave

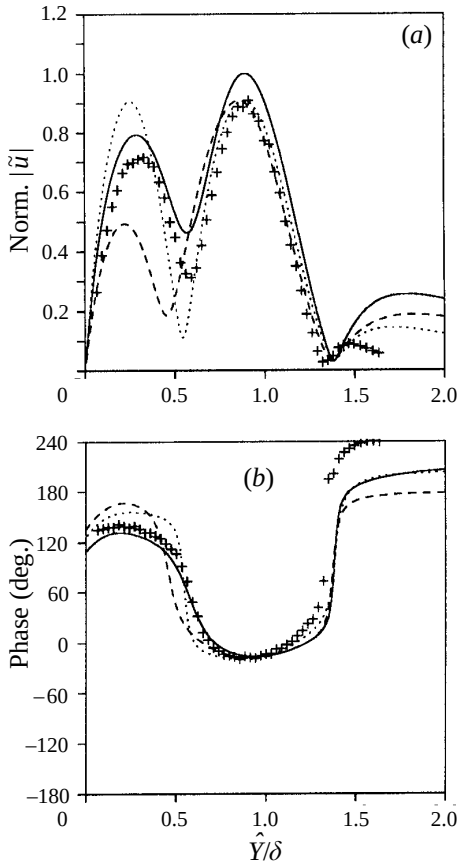

FIGURE 16. The amplitude and phase cross-stream distributions of $\tilde{u}$ at $R_j = 466$, $\gamma = 1.7$ and $\hat{X}/H = 30$. The symbols correspond to the experimental data, the dotted lines to the theoretical distributions of the viscous mode, the dashed lines to the theoretical distributions of the inviscid mode and the solid lines to the theoretical distributions based on the weighted contributions of both modes.

with downstream distance, the upstream-integrated contribution of the inviscid mode cannot be neglected. Therefore, at distances close to the upper branch (with respect to $\tilde{\beta}$) of region II, we expect the contribution of both modes to be significant and only further downstream should the viscous mode prevail.

The measured amplitude distributions of the streamwise velocity disturbance at three downstream locations are shown in figure 17(*a–c*) and compared with theoretical computations. In these experiments the jet-exit velocity and height were $3\,\mathrm{m\,s^{-1}}$ and 0.9 mm, respectively, the forcing frequency was 40 Hz and blowing with $\gamma = 1.5$ was applied. In accordance with the prediction of the linear theory, below region II ($\hat{X}/H = 30$) the experimental data fit the theoretical distribution of the inviscid mode, while at $\hat{X}/H = 70$, much above region II (high $\tilde{\beta}$), the viscous mode dominates. Both modes become significant just above region II ($\hat{X}/H = 40$) where only a proper decomposition of their weighted contributions (the solid line in figure 17*b*) can recover the experimental eigenfunction. The downstream growth of both modes (see figure

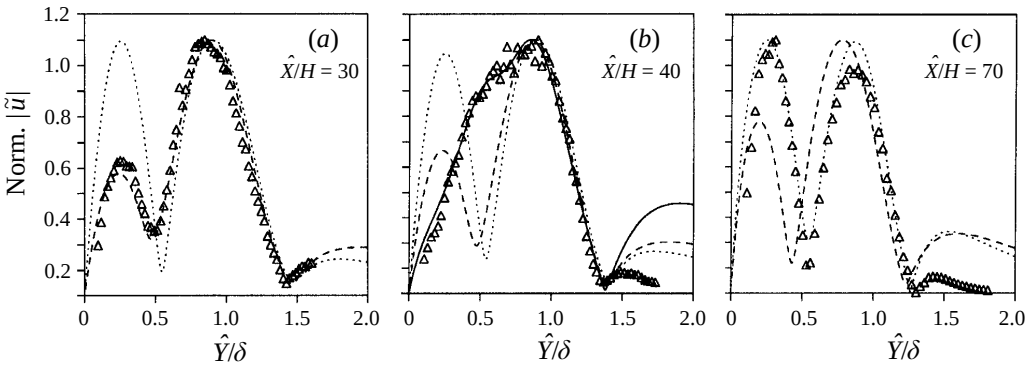

FIGURE 17. The amplitude cross-stream distributions of $|\tilde{u}|$ at $R_j = 270, \gamma = 1.5$ and three downstream locations. The symbols correspond to the experimental data, the dotted lines to the theoretical distributions of the viscous mode, the dashed lines to the theoretical distributions of the inviscid mode and the solid lines to the theoretical distributions based on the weighted contributions of both modes.

18) approximately follows the trends predicted by the linear stability theory. Similar results (not shown here) were obtained for the Glauert wall condition.

5. Summary and conclusions

This paper, focused on the development of the two instability modes during the initial stages of transition and on understanding how small amounts of blowing and suction can be used to control their relative dominance. In this section we first discuss some of the observations found in this work and when possible relate them to previous studies. We then summarize the effects of a small amount of wall blowing and suction on the evolution of the two instability modes.

During the initial stages of transition, the disturbed flow field of the wall jet consists of a double row of counter-rotating vortices, associated with the wall jet's inner and outer shear layers (Bajura & Catalano 1975; Gogineni *et al.* 1993; Hsiao & Sheu 1994). This vortical structure is reflected in the theoretical and experimental cross-stream distributions of the disturbance streamwise velocity of the inviscid and viscous modes. In the phase distribution of their streamwise velocity fluctuations (see the dotted and dashed lines in figure 14*b*) there are two approximately 180° sharp jumps, whereas the corresponding amplitude distributions (figure 14*a*) include three maxima. Similar experimental distributions were observed by Tsuji *et al.* (1977) and Zhou, Rothstein & Wygnanski (1992). The locations of the two sharp jumps in phase correspond to distances from the wall where the streamwise fluctuation changes sign and the cross-stream fluctuation reaches its maximum amplitude. Thus, together with the locations of zero velocity dictated by the boundary conditions at the wall and far away from it, the cross-stream distribution of the streamwise velocity fluctuation has four minima and three maxima. The two inner maxima are significantly larger than the outer one and their locations are approximately at distances from the wall where the phase velocity of the disturbance equals the local streamwise mean velocity.

The stability map of the wall jet includes three distinct regions: region I where only a single mode is unstable, region II where two unstable inviscid and viscous modes correspond to low- and high-frequency bands, respectively, and region III where the

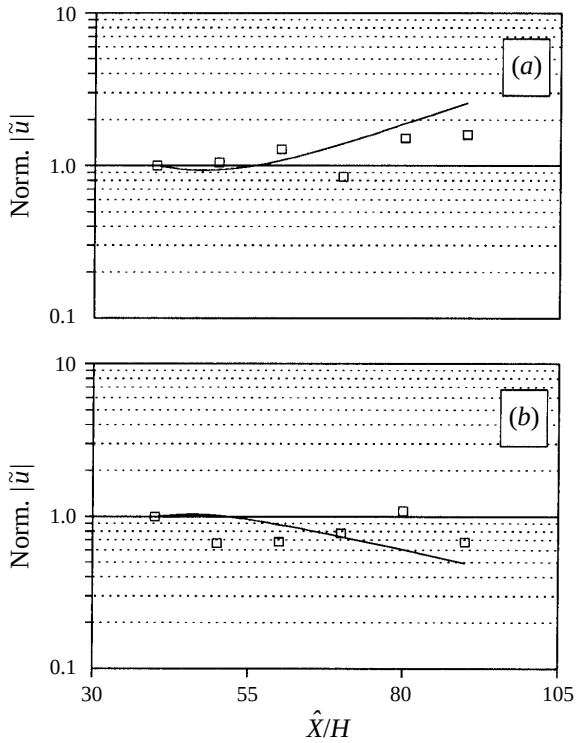

FIGURE 18. Comparison between the measured (symbols) and theoretical (solid lines) downstream development of (*a*) the viscous mode and (*b*) the inviscid mode of $|\tilde{u}|$ measured at $R_j = 270$, $\gamma = 1.5$ and $\hat{Y} = \hat{Y}_{55}$.

two bands of unstable modes have an overlapping region in which two waves have the same frequency, but different eigenvalues.

In accordance with the theoretical calculations, phase-locked experimental data, obtained when the wall jet was subjected to two-dimensional excitations, show that for large-scale disturbances the maximum of the amplitude distribution is at the outer region, while for small-scale disturbances the maximum is close to the wall. These results suggest that the small-scale disturbances are associated with the viscous boundary layer mode, while the large-scale ones are associated with the outer inviscid shear layer.

The possibility of the co-existence of the two instability modes was supported experimentally by Cohen *et al.* (1992) in natural jets and by Zhou *et al.* (1992) using phase-locked measurements in forced wall jets. In the latter case, however, the authors were able to follow the evolution of only a pure mode (inviscid or viscous) over a limited spatial distance by a careful selection of the parameters in their experiment. In this paper, using the decomposition method proposed by Tumin *et al.* (1996) we were able to uncouple the two modes and follow their evolution throughout the various regions of the stability map, and in particular across region III and across region II where the flow is dominated by both modes.

Theoretical cross-stream distributions of the streamwise disturbance, calculated for the various regions of the stability map, agree very well with phase-locked experimental data. The experimental data follow the trends predicted by the linear stability theory, according to which the ratio between the inner and outer maxima

of the streamwise eigenfunctions increases with downstream distance, while the ratio between the width of the disturbed region and the local boundary layer thickness decreases. These results are related to the increase of the non-dimensional frequency with downstream distance.

In order to compare the measured streamwise amplification of the disturbance with the theoretical prediction, the method of multiple scales was used to account for the mean flow divergence and to describe the growth of a two-dimensional wave disturbance in wall-jet flows. For this purpose, the second-order corrections to the mean flow solutions had to be obtained for all wall conditions. It should be noted that for the Blasius laminar boundary layer, the second-order corrections can be neglected. The mean flow divergence of the wall jet has a significant effect on the downstream evolution of a wavy disturbance having a fixed frequency. This is a result of the relatively strong streamwise variation of the corresponding non-dimensional frequency. For example, for a wall-jet flow over a solid surface ($\gamma = 2$), the non-dimensional frequency varies as $\sim \hat{X}^{5/4}$, two and a half times its rate in a laminar boundary layer over a flat plate.

A quantitative comparison between the theory and experiment shows that the downstream growth of the streamwise velocity fluctuations is well predicted by the theory only when the flow is dominated by a single mode (inviscid or viscous). When both modes co-exist in the flow, the agreement between the theoretical and experimental results is in general reasonable (excluding the case presented in figure 15*a*), but not as good as the case in which a single mode dominates the flow. The reason for this might be the limited ability of the bi-orthogonal decomposition method to precisely resolve the experimental signals into the respective contributions of the two modes. In this regard, it should be noted that the decomposition method assumes that the mean flow is parallel and that only two modes are present in the flow.

In the case associated with the streamwise evolution of the viscous mode across region III (see figure 15*a*), there is a severe difference between the experimental data and the theoretical prediction which follow opposite trends. In an attempt to explain this disagreement we note that among the various sets of experiments reported in this paper, the set associated with figure 15(*a*), is the one in which the highest jet-exit velocity ($7\,\mathrm{m\,s^{-1}}$) and dimensional excitation frequency (180 Hz), were used. We suspect that under these relative extreme experimental conditions, the screen used as the jet's wall was no longer at rest, but weakly forced to vibrate at the high excitation frequency. Consequently, there was some kind of interaction between the vibrating screen and the short-wavelength viscous mode which led to its rapid streamwise growth. In the future we plan to investigate this type of interaction.

In order to control the relative dominance of each of the instability modes, the wall jet was subjected to a small amount of wall blowing and suction. Mean flow calculations and measurements show that the direct effect of the wall suction and blowing is to increase and decrease, respectively, the slope of the streamwise mean velocity profile at the wall. Consequently, as predicted by the linear stability theory and confirmed experimentally, blowing and suction tend to increase and decrease, respectively, the ratio between the outer and inner amplitude maxima of the streamwise velocity fluctuation.

Measurements obtained in natural and forced wall jets confirm the theoretical predictions that the initial growth of the viscous mode is higher when blowing is applied and lower when suction is applied, whereas the bandwidth of frequencies associated with the the unstable viscous mode is wider for blowing and narrower for suction. In addition, when blowing is applied the region where both unstable modes

co-exist begins at a lower local Reynolds number. This, together with the fact that blowing destabilizes the short-wavelength viscous mode (see figure 3*a*), might explain the rapid transition observed in natural wall-jets subjected to wall blowing (see figure 6). Opposite effects are caused when suction is applied.

The authors are grateful to Mr A. Beer for designing and constructing the apparatus. The authors would also like to thank Dr V. Levinski for his help in solving the second-order mean flow problem and Dr J. Tanny for his careful reading of the manuscript and helpful comments. This research was supported by grant no. 88-00228 from the United States–Israel Binational Science Foundation (BSF), Jerusalem, Israel and by Technion V.P.R. Fund— J. and J. Gringorten Aeronautical Research Fund.

Appendix

In this Appendix, the second-order correction to the wall-jet mean flow solution, when the jet is subjected to wall suction or blowing, is obtained. This solution is a generalization of the second-order solution found by Plotkin (1970) for the Glauert wall jet. The equation for the two-dimensional stream function ψ is given by

$$\left[\psi_y(\partial/\partial x) - \psi_x(\partial/\partial y) - (1/R)\nabla^2\right]\nabla^2\psi = 0, \tag{A 1}$$

where R is the Reynolds number based on an arbitrary reference velocity, U_r, and length scale, L_r, which were used to render all variables dimensionless. Using the method of matched asymptotic expansions (Van Dyke 1975), we assume straightforward expansions for the outer inviscid and inner viscous fields, respectively.

First-order problem

Since the upstream outer flow is negligible, the first term of the outer inviscid expansion is zero. Consequently, an outer expansion, valid outside the jet, is assumed as

$$\psi(x, y; R) = 0 + \delta_2(R)\psi_2(x, y) + \ldots. \tag{A 2}$$

In order to satisfy the inner boundary conditions, the following inner expansion, valid within the jet, is assumed:

$$\psi(x, y; R) = R^{-1/2}\Psi_1(x, Y) + R^{-1}\Psi_2(x, Y) + \ldots \tag{A 3}$$

where $Y = R^{1/2}y$. The equation for Ψ_1 is

$$\Psi_{1YYY} + \Psi_{1x}\Psi_{1YY} - \Psi_{1Y}\Psi_{1xY} = 0, \tag{A 4}$$

and the boundary conditions are

$$\Psi_{1Y}(x, 0) = 0, \quad -\Psi_{1x}(x, 0) = V_w(x) \quad \text{and} \quad \Psi_{1Y}(x, \infty) = 0, \tag{A 5}$$

where V_w is the normal velocity at the wall.

A similarity solution for Ψ_1 has been found by Cohen *et al.* (1992). Accordingly,

$$\Psi_1(x, Y) = x^{1-b}f(\eta) \quad \text{where} \quad \eta = (1-b)Y/x^b. \tag{A 6}$$

The reduced equation for f is

$$f''' + ff'' + \gamma f'^2 = 0, \tag{A 7}$$

where

$$\gamma = \frac{2b-1}{1-b}, \tag{A 8}$$

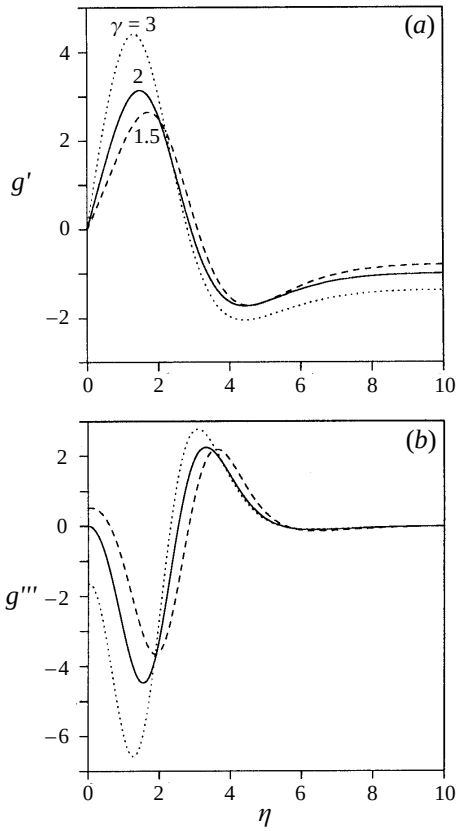

FIGURE 19. (*a*) First and (*b*) third derivatives of second order viscous mean stream function calculated for three values of γ.

and the appropriate boundary conditions are

$$f'(0) = f'(\infty) = 0 \quad \text{and} \quad f(0) = f_0, \tag{A 9}$$

where

$$f_0 = \frac{x^b V_w(x)}{b-1}. \tag{A 10}$$

The self-similar solutions differ from one another only in the constant γ. According to its value the solutions can be divided into three cases: suction when $\gamma > 2$, the Glauert solution with $\gamma = 2$ and blowing when $1 < \gamma < 2$.

Second-order outer problem

The first-order inner viscous solution induces a correction in the outer inviscid solution. Matching of the outer expansion with the first-order inner viscous solution yields $\delta_2(R) = R^{-1/2}$ and $\psi_2(x,0) = \Psi_1(x,\infty) = x^{1-b} f(\infty) = x^{1-b}$. In addition, the upstream condition for ψ_2 is that $\psi_2(x,0) = 0$ for $x < 0$. Thus, the solution of ψ_2, which satisfies the Laplace equation subjected to the above boundary conditions, is

$$\psi_2(x,y) = \mathrm{Re}\left[(x+\imath y)^{1-b}\right] + a\,\mathrm{Im}\left[(x+\imath y)^{1-b}\right], \tag{A 11}$$

where Re and Im denote the real and imaginary parts, respectively, and

$$a = -\cot\left[\pi(1-b)\right]. \tag{A 12}$$

The second-order outer solution found by Plotkin (1970) for the Glauert wall jet ($b = 3/4$) is a member of this family of solutions with $a = -1$.

Second-order jet solution

The equation for Ψ_2 is

$$\Psi_{2YYY} + \Psi_{1x}\Psi_{2YY} - \Psi_{1Y}\Psi_{2xY} + \Psi_{2x}\Psi_{1YY} - \Psi_{2Y}\Psi_{1xY} = 0. \tag{A 13}$$

The boundary conditions at the wall are $\Psi_2(x,0) = \Psi_{2Y}(x,0) = 0$. The third outer boundary condition $\Psi_{2Y}(x,\infty) = a(1-b)x^{-b}$ is obtained by matching with the second-order outer solution. In the search for similarity solutions, the form $\Psi_2(x,Y) = g(\eta)$ is assumed and the resulting second-order inner problem is

$$g''' + fg'' + \frac{3b-1}{1-b} f'g' = 0, \tag{A 14}$$

with the boundary conditions

$$g(0) = g'(0) = 0, \quad g'(\infty) = a. \tag{A 15}$$

The equation has been solved numerically using a fourth-order Runga–Kutta subroutine. The results for g' and g''', which are used in obtaining the effect of the mean flow divergence on the growth of the disturbance, are shown in figures 19(a) and 19(b), respectively, for $\gamma = 1.5, 2$ and 3.

REFERENCES

Akatnov, N. I. 1953 Development of two-dimensional laminar incompressible jet near a rigid wall. *Proc. Leningrad Polytech. Inst.* **5**, 24.

Amitay, M. 1994 Theoretical and experimental investigation of a laminar two-dimensional wall-jet. PhD Thesis, Faculty of Aerospace Engineering, Technion, Israel.

Amitay, M. & Cohen, J. 1993 The mean flow of a laminar wall-jet subjected to blowing or suction. *Phys. Fluids* A **5**, 2053.

Bajura, R. A. & Catalano, M. R. 1975 Transition in a two-dimensional plane wall jet. *J. Fluid Mech.* **70**, 773.

Bajura, R. A. & Szewczyk, A. A. 1970 Experimental investigation of a laminar two-dimensional plane wall jet. *Phys. Fluids* A **13**, 1653.

Bouthier, M. 1973 Stabilité linéair des écoulements presque parallèles. Part II. Lacouche limit de Blasius. *J. Mec.* **12**, 75.

Chun, D. H. & Schwarz, W. H. 1967 Stability of the plane incompressible viscous wall jet subjected to small disturbances. *Phys. Fluids* A **10**, 911.

Cohen, J. 1994 The initial evolution of a wave packet in a laminar boundary layer. *Phys. Fluids* **6**, 1133.

Cohen, J., Amitay, M. & Bayly, B. J. 1992 Laminar-turbulent transition of wall jet flows subjected to blowing and suction. *Phys. Fluids* A **4**, 283.

Fazel, H. & Konzelmann, U. 1990 Non-parallel stability of a flat-plate boundary layer. *J. Fluid Mech.* **221**, 311.

Gaster, M. 1962 A note on the relation between temporally-increasing and spatially-increasing disturbances in hydrodynamic stability. *J. Fluid Mech.* **14**, 222.

Gaster, M. 1974 On the effects of boundary-layer growth on flow stability. *J. Fluid Mech.* **66**, 465.

Glauert, M. B. 1956 The wall-jet. *J. Fluid Mech.* **1**, 625.

Glauert, M. B. 1958 In Boundary Layer Research Symposium (ed. by H. Görtler), p. 72. Springer.

Gogineni, S., Shih, C. & Krothapalli, A. 1993 PIV study of a two-dimensional transitional wall jet. *Paper AIAA* 93-2913.

Hsiao, F. B. & Sheu, S. S. 1994 Double row vortical structures in the near field of a plane wall-jet. *Exps. Fluids* **17**, 291.

Mele, P., Morganti. M., Scibilia, M. F. & Lasek, A. 1986 Behavior of wall jet in laminar-to-turbulent transition. *AIAA J.* **24**, 938.

Nayfeh, A. H. & Padhye, A. 1979 Relation between temporal and spatial stability in three-dimensional flows. *AIAA J.* **17**, 1084.

Plotkin, A. 1970 A second-order correction to the Glauert wall jet solution. *AIAA J.* **8**, 188.

Saric, W. S. & Nayfeh, A. H. 1975 Nonparallel stability of boundary-layer flows. *Phys. Fluids* **18**, 945.

Shih, C. & Gogineni, S. 1993 Vortex/boundary layer interaction of a wall jet. *Pacific Intl Conf. on Aerospace Sciences Meeting, December, Tainan, Taiwan, ROC.*

Tetervin, N. 1948 Laminar flow of a slightly viscous incompressible fluid that issues from a slit and passes over a flat plate. *NACA TN* 1644.

Tsuji, Y. N., Morikawa, Y., Nagatani, T. & Sakou, M. 1977 The stability of a two-dimensional wall jet. *Aero. Q.* **28**, 235.

Tumin, A. M., Amitay, M., Cohen, J. & Zhou, M. D. 1996 A normal multi mode decomposition method for stability experiments. *Phys. Fluids* **8**, 2777.

Van Dyke, M. 1975 *Perturbation Methods in Fluid Mechanics.* The Parabolic Press.

Zhigulev, V. N. & Tumin, A. M. 1987 *Origin of Turbulence.* Novosibirsk, Nauka (In Russian).

Zhou, M. D., Rothstein, J. & Wygnanski, I. 1992 On the hydrodynamic stability of the wall jet. *11th Australian Fluid Mechanics Conf., Univ. of Tasmania, Hobart, Australia, 14–18 December.*